Cystin is required for maintaining fibrocystin (FPC) levels and safeguarding proteome integrity in mouse renal epithelial cells

Running title: Cystin deficiency reduces FPC levels through enhanced autophagic degradation.

Yiming Zhang[1#], Chaozhe Yang[2], Wei Wang[3], Naoe Harafuji[2], P. Darwin Bell[4], Ljuba Caldovic[2], Lisa M. Guay-Woodford[2,5*] and Zsuzsanna Bebok[1*]

1. University of Alabama at Birmingham, School of Medicine, Department of Cell Developmental and Integrative Biology (CDIB).
2. Center for Translational Research, Children's National Hospital, Washington, DC.
3. University of Alabama at Birmingham, School of Medicine, Cystic Fibrosis Research Center
4. University of Alabama at Birmingham, Department of Medicine, Division of Nephrology.
5. Center for Genetic Medicine Research, Children's National Hospital, Washington DC.

*To whom correspondence should be addressed.

LGW: lguaywoo@childrensnational.org

ZsB: bebok@uab.edu

[#]Current contact for Yiming Zhang: ymjzhang@mit.edu

ABSTRACT

Autosomal recessive polycystic kidney disease (ARPKD) is primarily caused by mutations in *PKHD1,* encoding fibrocystin (FPC). Recently, patients with *CYS1 mutations*, encoding cystin, have also been identified. While *Pkhd1* mutant mice do not exhibit ARPKD-like phenotype, cystin deficient *Cys1*$^{cpk/cpk}$ (*cpk*) mice do. We explored potential functional interactions between FPC and cystin in mouse kidneys and cortical collecting duct (CCD) cell lines. FPC levels were markedly reduced in both *cpk* kidneys and CCD cells through selective autophagy. Re-expression of *Cys1* in *cpk* kidneys restored and siRNA silencing of *Cys1* in wild type-CCD cells reduced FPC levels. In contrast, FPC deficiency in *Pkhd1* mutant kidneys did not diminish cystin levels. Consistent with the previously identified role of FPC in E3 ubiquitin ligase complexes (NEDD4), we observed reduced polyubiquitination with elevated epithelial sodium channel (NEDD4 target) levels and function in *cpk*-CCD cells. Our results imply that cystin stabilizes FPC in E3-ligase complexes and helps to maintain proteome integrity. In *cpk* mice, cystin loss causes increased MYC expression and also leads to severe FPC reduction and altered proteome. Together these perturbations promote cystogenesis. We speculate that in *Pkhd1* mutants FPC loss alone is insufficient for kidney cyst formation, because cystin prevents *c-Myc* overexpression.

INTRODUCTION

The C57BL/6J*Cys1*$^{cpk/cpk}$ (*cpk*) mouse is the first described experimental model of polycystic kidney disease (PKD) (1), in which a spontaneous mutation in the gene *Cys1* (encoding the protein cystin) causes renal cystic disease that phenocopies human ARPKD (2). In contrast, causative mutations in the majority of ARPKD patients occur in *PKHD1*, encoding fibrocystin (FPC) (3). Recently, patients with ARPKD, linked to mutations in *CYS1* have been identified (4). It is not understood why mutations in *CYS1 (Cys1)* and *PKHD1* lead to similar kidney phenotypes. While a physical interaction between cystin and FPC could not be demonstrated, a functional interplay among these proteins may be essential during kidney development and when disrupted, renal cystic disease occurs. We therefore sought to identify potential functional linkages between cystin and FPC in mouse kidneys (4) and cortical collecting duct (CCD) cell lines (5, 6).

The *cpk* phenotype is caused by a frameshift mutation within *Cys1* exon 1, leading to reduced *Cys1* mRNA levels and consequent loss of cystin, a hydrophobic, 145-amino acid, N-terminally myristoylated protein (7). In mouse renal epithelial cells, cystin traffics to the primary cilium and co-localizes with other PKD-associated proteins including polaris/Ift88 (8). N-myristoylation modulates protein plasma membrane association and impacts protein function via subcellular trafficking and localization (9-13). Cystin, myristoylated on amino acid (AA) residue G2, localizes to lipid raft membrane microdomains (14). Myristoylation and a short peptide sequence encoded between AAs 28 to 35 (AxEGG) are both required for cystin trafficking to, and retention in, the primary cilium (15). Cystin also localizes to the cell nucleus in a regulatory complex with necdin (15). In the absence of cystin, necdin activates *Myc* transcription. Importantly, c-Myc levels are significantly elevated in both *PKHD1* mutation-associated ARPKD kidneys and mouse *cpk* cystic kidney cells (15). Furthermore, dysregulated *Myc/MYC* expression has been implicated as a central driver of PKD (16, 17).

In contrast to *cpk* mice, *Pkhd1* mutants fail to develop an ARPKD-like renal phenotype (18). FPC, encoded by Pkhd1, is a large transmembrane protein with a long extracellular N-

terminus and a short cytoplasmic C-tail (18, 19). Although the function of FPC is largely unknown, it is required for the function of HECT domain-containing E3 family ligases and co-localizes in vesicles with the NEDD4 ubiquitin ligase interacting protein, NDFIP2 (20). FPC deficiency is associated with enhanced activity of ENaC, a NEDD4 target protein (21) and dysregulation of which may contribute to the systemic hypertension that is characteristic of ARPKD (22, 23). While the current studies were not designed to directly address the discordant renal phenotypes observed in *PKHD1*-associated human ARPKD and mouse *Pkhd1* mutants, we propose that a mechanistic understanding of potential interactions between cystin and FPC in mouse renal epithelial cells may shed light on relevant mechanistic pathways that contribute to cystogenesis in human *PKHD1*-associated kidney disease.

In the present study, we examined cystin and FPC levels in the kidneys of *wt*, *Pkhd1* mutant mice (18); *cpk* and rescued *cpk* (r-*cpk*) mice with collecting duct specific expression of a wild-type *Cys1* transgene (4). FPC was severely reduced (approximately 90%) in *cpk* compared to *wt* kidneys, but FPC levels increased by the re-expression of a *wt Cys1* transgene. On the contrary, FPC loss did not alter cystin levels in *Pkhd1* mutants. Using renal cortical collecting duct (CCD) cell lines generated from *wt* and *cpk* mouse kidneys (5, 6), we observed that in cystin deficient-cells, FPC levels were reduced through an autophagic mechanism. This autophagic reduction of FPC led to reduction of ubiquitination to a level that is likely to alter cellular proteome. As would be expected based upon previously reported dysregulation of the NEDD4-family of HECT-domain E3 ligases in *Pkhd1* mutant cells (20), ENaC levels were higher in *cpk* cells with reduced FPC levels and transepithelial sodium transport was increased, consistent with reduced turnover of this NEDD4 target protein (24) .

Based on our observations, we propose that cystin stabilizes FPC in E3-ligase complexes, protecting FPC from rapid autophagic degradation and thereby helping to maintain cellular proteome integrity. The ARPKD-like renal cystic phenotype in *cpk* mice results from the combined loss of FPC leading to proteome alterations that disrupt cellular homeostasis, and c-myc

overexpression due to loss of cystin-dependent negative regulation of *Myc* transcription (15). Identification of a functional connection between cystin and FPC leads us to suggest that in *Pkhd1* mutant mice, the presence of cystin prevents the development of the ARPKD-like renal cystic phenotype because cystin constrains *Myc* transcription (15).

RESULTS

I. Lack of cystin leads to reduced FPC levels

Cystin deficiency is associated with marked reduction of FPC in *cpk* mouse kidneys. We hypothesized that similar *CYS1*/*Cys1* and *PKHD1* renal disease phenotypes might reflect disruption of an essential functional interaction between cystin and FPC. To test this hypothesis, we compared FPC and cystin levels in the kidneys of *wt*, *cpk* and r-*cpk* mice (rescued with collecting duct-specific expression of the *Cys1-GFP* transgene) ***(Fig.1A).*** Our results showed a marked (90%) reduction ***(Fig.1B)*** of FPC in *cpk* kidneys compared to *wt*, and we observed a significant increase of FPC in r-*cpk.* FPC was not restored to *wt* levels in whole r-*cpk* kidney lysates, but rather reflects collecting duct-specific expression of the *Cys1-GFP* transgene. Cystin was present in *wt* but not in *cpk* kidney, and we confirmed high levels of cystin-GFP in r-*cpk* kidney lysates ***(Fig.1A, lower panel)***. Measurement of *Pkhd1* mRNA levels in the kidneys of *wt* and *cpk* mice indicated a slight (~1.5-fold) increase in *cpk* cells compared to *wt,* suggesting that cystin-dependent FPC downregulation occurred at the protein level ***(Fig.1C)***. In order to determine if cystin levels are dependent on FPC expression, we analyzed *Pkhd1* mutant kidneys (*del3-4, del67, del3-67*) for cystin and FPC expression ***(Fig.1D)***, observing that loss of FPC was not associated with reduced cystin levels. Therefore, loss of cystin influenced FPC levels, but cystin abundance was not affected by reduced FPC protein expression.

FPC levels are linked to cystin expression in cortical collecting duct (CCD) cell lines. For the subsequent mechanistic studies, we used cell lines developed from *wt* and *cpk* mouse CCD cells (5, 6). To validate these lines, we evaluated the expression of the epithelial cell marker, e-

cadherin, and the CCD marker, AQP2 (25). We found similar levels of e-cadherin and AQP2 in *wt* and *cpk* cells ***(Fig.2A,B).*** As expected, cystin was present in *wt*, but absent from *cpk* cells ***(Fig.2C)***. Similar to our observation in whole kidneys, FPC levels were greatly reduced (83 ± 6 %) in *cpk* cells ***(Fig.2D)***. To determine whether the impact of cystin deficiency was FPC-specific or generalizable to other ciliary and PKD-associated proteins, we examined levels of the proteins polycystin-2 (Pc2) and Ift88, which were previously shown to colocalize with cystin (7). Pc2 reduction was significant (30±6 %) in *cpk* cells ***(Fig.2D)***, consistent with a previous report that FPC removal reduces Pc2 levels (26). However, there was no effect on Ift88 ***(Fig.2E)***. These results support a specific relationship between cystin and FPC expression, as we observed in kidneys. *Pkhd1* mRNA levels in *wt* and *cpk* cells were similar (***Fig.2F)***, supporting our hypothesis that cystin affects FPC abundance at the protein level.

To further confirm a role for cystin in maintaining FPC levels, we used siRNA to reduce *Cys1* expression in *wt* cells. We achieved siRNA dose-dependent (20-80 ng/ml) reductions in cystin levels following 72 hours of siRNA transfection ***(Fig.3A,B)***, and reduction of FPC correlated with the efficiency of *Cys1* knockdown. Taken together, our *in vivo* and *in vitro* observations strongly support a role for cystin in maintaining FPC levels in renal epithelial cells.

II. The mechanism of FPC loss in *cpk* cells.

Selective autophagy as a pathway for FPC removal in *cpk* cells. Similar *Pkhd1* mRNA levels in *wt* and *cpk* kidneys as well as in CCD cells (***Fig.1-2)*** implied that FPC loss was not the result of reduced *Pkhd1* transcription or mRNA stability, but occurred at the protein level. If cystin plays an essential role in maintaining FPC levels, we reasoned that in the absence of cystin, FPC should undergo degradation, through one of the intracellular protein degradation pathways (*i.e.* proteasomes, lysosomes, or selective autophagy).

We first examined whether cystin was involved in directing FPC trafficking by binding to the cytosolic side of FPC-containing vesicles. In this case, cystin absence would lead to FPC mistargeting and subsequent degradation. In *wt* cells we were unable to detect colocalization of cystin with FPC-containing vesicles ***(Fig.4A, left panels).*** In *cpk* cells, as expected, cystin was undetectable and FPC was very low ***(Fig.4A, right panels).*** The absence of vesicle-associated cystin-FPC colocalization argued against cystin functioning as an escort protein of FPC-containing vesicles.

Alternatively, loss of FPC might occur at the ER membrane, through endoplasmic reticulum-associated degradation (ERAD). FPC is a glycoprotein with multiple N-glycosylation sites that undergo complex glycosylation during its passage through the Golgi. Therefore, if FPC was retained in the ER and removed by ERAD, some of the remaining FPC in *cpk* cells would have a lower molecular weight, reflecting core glycosylation. However, our WB data demonstrate the same MW of full length FPC in *wt* and *cpk* kidneys and CCD cells, suggesting that FPC in *cpk* cells trafficked through the Golgi ***(Fig.1-2)***. In addition, proteasome inhibition (MG-132) for four hours did not result in increased levels of the core glycosylated, ER form of FPC in *cpk* cells, suggesting that FPC reduction in *cpk* cells does not involve ERAD ***(Fig.4B).*** We further observed that prolonged treatment with MG132 (for 8h) did not lead to increased FPC levels, but rather caused a severe *reduction* of FPC, not only in *cpk* but also in *wt* cells ***(Fig.5B)***. Notably, extended proteasome inhibition has been shown to activate autophagy as an alternative pathway for protein degradation (27-29).

We also tested both chloroquine (CQ) and bafilomycin (BF) to determine whether lysosome inhibition (LI) affected FPC abundance and found that neither agent altered FPC levels in either *wt* or *cpk* cells. These data suggested that FPC was degraded through selective autophagy, as has been reported for other ciliary proteins (30, 31)

Prior studies have shown that FPC itself is a functional component of the NEDD4-family of E3 ubiquitin ligase complexes that facilitate the ubiquitination of multiple proteins (20), and that

a lack of FPC compromised the function of intracellular protein degradation systems. Therefore, in *cpk* cells with minimal FPC levels, ubiquitination could be compromised, a condition which can itself lead to the activation of alternative protein degradative pathways, including selective autophagy (27, 32).

To test whether selective autophagy was activated in *cpk* cells, we used SQSTM1/p62 as a reporter for selective autophagy. SQSTM1/p62 links the autophagy receptor LC3 with ubiquitinated proteins (33-35) to regulate autophagic degradation and cytoplasmic segregation of ubiquitinated proteins (36-38). When autophagic flux is acutely activated, SQSTM1/p62 levels decrease. By contrast, compromised protein degradation, such as that associated with upregulation of selective autophagy as an alternative degradation pathway, rapidly upregulates SQSTM1/p62 levels (39). Consistent with these reports, we observed elevated SQSTM1/p62 expression in *cpk* cells compared to *wt* ***(Fig.5A),*** suggesting a state of compromised protein degradation in *cpk* cells with minimal levels of FPC.

Prolonged proteosome inhibition (PI) can induce autophagy as an alternative protein degradation pathway (27-29). Furthermore, LI using CQ or BF can also inhibit the late steps of autophagy by hindering the fusion of lysosomes with autophagic particles in which proteins are sequestered (40), or impairing V-ATPase-dependent acidification of lysosomes, respectively (41-43). We therefore measured levels of SQSTM1/p62 in control, PI and LI-treated cells. In *wt* cells, p62 levels increased following both PI and LI, consistent with activation of autophagy as an alternative protein degradation pathway, Notably, *cpk* cells exhibiting higher baseline levels of p62 also had p62- oligomers, indicative of autophagy hyperactivation under PI and LI inhibition ***(Fig.5C)*** (44). Using western blotting, we analyzed the soluble fraction of cellular proteins, and showed that PI led to a reduction in FPC without affecting other cystoproteins including Pc2 and Ift88, or total proteins stained with REVERT ***(Fig.5B,D)***. These observations indicate that extended PI led to targeting of FPC to selective autophagy ***(Fig.5D)***.

We used confocal microscopy to determine whether FPC was present in cytosolic autophagic particles under the above experimental conditions. We induced autophagy by PI and treated cells with CQ to inhibit lysosomes, thereby preventing degradation of proteins before they fuse with lysosomes ***(Fig.6).*** Under these conditions, in *wt* cells we observed large cystin-containing particles, some of which also contained FPC. In *cpk* cells, which lack cystin and have reduced FPC, we detected FPC only in some cells. These results are consistent with the selective autophagic degradation of FPC that is activated in the absence of cystin.

III. The consequences of cystin and FPC loss in *cpk* cells

Reduced ubiquitination in *cpk* cells. The NEDD4 family of E3 ligases belong to the homologous to E6AP C-terminus (HECT) domain E3 ligase group, which regulate multiple cellular activities through protein ubiquitination (for review: (45)). E3 ligases facilitate multiple types of ubiquitination (46) ***(Fig. 7A).*** FPC deficiency-associated E3 ligase dysfunction in *cpk* cells should, therefore, result in altered polyubiquitination of numerous proteins, hinder the ubiquitin proteosome system (UPS) and lysosomal degradative systems, disrupting proteome homeostasis. We examined whether reduced FPC (83% less than *wt*) in *cpk* cells affected polyubiquitination in general. We used linkage-specific anti-ubiquitin antibodies (47) to compare levels of polyubiquitination in *wt* and *cpk* cells, following PI. While PI led to increased ubiquitination in both cell lines, polyubiquitination was lower in *cpk* cells compared to *wt* (***Fig. 7B)***. To determine which type of ubiquitination was affected, we used anti-ubiquitin antibodies recognizing all types of polyubiquitin links (Pan-ubi), K48-linked ubiquitin, and K63-linked ubiquitin. *Cpk* cells exhibited reduced levels of total polyubiquitination ***(Fig. 7B),*** K63-linked ***(Fig. 7C),*** and K48-linked polyubiquitin chains ***(Fig.7D).*** These results are consistent with reduced HECT E3 ligase activity in *cpk* cells, that may impede protein quality control, cellular signaling, and proteome homeostasis (45).

Enhanced expression of the epithelial sodium channel (ENaCα) in *cpk* cells. Because abnormal proteome homeostasis resulting from reduced HECT domain E3 ligase activity and

ubiquitination can impact cell surface receptors and transporters (45), we examined the expression and function of the epithelial sodium channel (ENaC), which is a substrate of the HECT domain, NEDD4 family of E3 ligases (21). Furthermore, ENaC was examined in this study because excessive renal ENaC activity is associated with high blood pressure (48, 49), and systemic hypertension is a hallmark of ARPKD (22, 50). Previous studies have demonstrated that expression of the functional alpha subunit of ENaC (ENaCα) is regulated via ubiquitination and degradation by both the UPS and lysosomes (24, 51, 52). We observed increased abundance of ENaCα in *cpk* compared to *wt* cells ***(Fig. 8A,B).*** Confocal microscopy confirmed higher membrane ENaC levels in *cpk* cells ***(Fig.8C)***, with strong vesicular ENaCα staining and significant co-localization with lysosome-associated membrane protein 1 (LAMP1), which delivers proteins to the lysosome ***(Fig.8D)***. In *wt* cells, ENaCα was mostly observed in vesicular compartments, and was not colocalized with LAMP1. Our observations suggest that ENaC turnover is reduced in *cpk* compared to *wt* cells, and are consistent with previous findings indicating that FPC deficiency is linked to reduced NEDD4 E3 ligase activity, leading to defective downregulation of cell surface transporters including ENaC (20).

Higher ENaCα levels correspond to enhanced sodium transport. To determine whether increased ENaCα membrane abundance actually correlated with increased sodium transport, we performed whole-cell patch analysis on *wt* and *cpk* cells (53, 54). Both cell types exhibited currents sensitive to the ENaC inhibitor amiloride ***(Fig. 9A-FC)***. We measured net amiloride-sensitive currents by subtracting the currents in the presence of amiloride from control currents ***(Fig.9C,F)*** and plotted the mean I-V relation of amiloride-sensitive currents from *wt* and *cpk* cells, respectively ***(Fig.9G,H)***. Mean I-V curves of absolute amiloride-sensitive currents from *cpk* cells showed higher amiloride-sensitive currents at each membrane potential compared to *wt*. At positive membrane potentials (from -10 to 30 mV) when the I-V relation was expressed by current density ***(***pA/pF, ***Fig.9H)***, we observed that *cpk* cells showed significantly larger amiloride sensitive

currents, suggesting that there are more fluxes of amiloride-sensitive currents in *cpk* cells. In addition, amiloride-sensitive currents from *cpk* cells are outward-rectified, in contrast to *wt* cells with inward rectified currents, contributing to high amiloride-sensitive currents from *cpk* cells at positive membrane potentials. Our findings indicate a positive correlation between higher ENaCα membrane abundance and enhanced amiloride-sensitive currents in *cpk* cells, a result consistent with the anticipated consequences of FPC deficiency-linked changes in proteome homeostasis.

DISCUSSION

Our studies demonstrate that in both mouse kidneys and CCD cell lines, loss of cystin led to an 80-90% reduction in FPC levels, which occurred at the protein level via selective autophagy. Both the natural mutation-mediated loss of cystin in *cpk* kidneys and CCD cells, as well as siRNA removal of *Cys1* mRNA in *wt* CCD cells led to FPC reduction. In contrast, collecting duct-specific expression of cystin in *cpk* mice (4) partially rescued FPC levels. Cystin-dependent FPC regulation is unidirectional because loss of FPC in *Pkhd1* mutant mouse kidneys did not affect cystin expression.

FPC deficiency led to reduced protein polyubiquitination. This is consistent with prior studies showing that FPC is a functional component of the HECT-domain NEDD4 family of E3 ubiquitin ligases (20). We hypothesized that such changes may alter the homeostasis of ENaC, a NEDD4 target protein (21). In this study, we observed elevated ENaC protein levels, upregulation of ENaC expression in the plasma membrane, and increased sodium transport in *cpk* cells, which supports our hypothesis and reveals a possible mechanism underlying the systemic hypertension that is a hallmark symptom of ARPKD (22, 50).

Selective autophagy was activated in cystin-deficient *cpk* cells at baseline, most likely by disturbances in E3 ligase function, which is necessary for proper protein quality control (for review:(45, 55)). Interestingly, autophagy hyperactivation led to the degradation of FPC not only

in *cpk* but also in *wt* cells, suggesting that FPC downregulation occurs through selective autophagy as has been shown for other PKD-associated proteins (30, 31).

We also demonstrated significant reduction in polyubiquitination, suggesting that in CCD cells, FPC plays a significant role in protein quality control and proteome management. Our data are consistent with the interactive feedback among intracellular protein degradation systems (proteasome, lysosomes and different types of autophagy) in maintaining cellular homeostasis. When one of these systems is rendered dysfunctional, other intact protein degradative pathways undergo dynamic adjustments to maintain proteome integrity (55). We propose that in the absence of cystin, FPC undergoes targeted degradation that renders the NEDD4 E3 ligase complex dysfunctional. The downstream consequences involve dismantling of the integrated protein quality control mechanisms that maintain cellular proteome integrity. This hypothesis is supported by previous studies reporting attenuated expression of epithelial adhesion molecules (56), altered basement membrane deposition (57), and metabolic abnormalities (5) in *cpk* cells.

Our studies show that a functional interaction of cystin and FPC is required for the physiological function of cellular protein degradation pathways in cells which express these proteins. Therefore, we extend the previously proposed role of FPC in maintaining the integrity of signaling pathways, protein quality control and turnover (18) upstream, to include cystin. We also determined, that cystin affects FPC abundance in a unidirectional manner, in that loss of FPC in *Pkhd1* mutant mouse kidneys was not associated with reduced cystin levels. This observation may be critically important for clarifying an otherwise apparent paradox. That is, why does the loss of FPC cause renal cysts in *cpk* but not *Pkhd1* mutant mice? We propose that, in mice, cystin has at least two essential roles by maintaining FPC as a required functional component of the NEDD4 E3 ligase complex, and inhibiting *Myc* expression via interaction with necdin, as we demonstrated previously (15). We propose that in mouse kidneys, more specifically in collecting duct epithelial cells, FPC loss and MYC overexpression together are required for cystogenesis. By contrast, *Pkhd1* mutant mice lacking FPC retain cystin levels (see Fig. 1) that can maintain

Myc expression inhibition through necdin interaction (15). We suggest that disruption of proteome homeostasis is a significant pathophysiological consequence of FPC loss, yet not sufficient for renal cyst formation in mice. Identification of all E3 ubiquitin ligases and the extent by which the cellular proteome is affected by the loss of FPC in mouse and human kidneys will require further investigations. Those studies will likely shed light on factors that are responsible for the differences observed between human and mouse kidney phenotypes following FPC loss.

Finding a functional link between cystin and FPC expression in collecting duct cells supports the use of the *cpk* mouse as an important experimental model to study ARPKD pathogenesis and experimental therapeutics. Our studies also provide novel perspectives on the renal phenotype in mouse models of ARPKD, suggesting that future studies should assess FPC and cystin levels, MYC expression, and cellular proteome status. Further, the recent identification of patients with *CYS1* mutations and an ARPKD-like renal phenotype adds potential importance of these findings to the development of novel therapeutic targeting for human disease.

MATERIALS AND METHODS

Mice: Kidney tissues were collected from gender matched, 14-days old animals. All animal procedures were approved by the Institutional Animal Care and Use Committees of Children's National Research Institute and the University of Alabama at Birmingham (UAB).

Analysis of kidney tissue lysates: Kidney tissue was collected, homogenized, and processed for immunoblotting as previously described (15). Immuno-reactive protein bands were visualized using SuperSignal West Dura chemiluminescent substrate (Thermo Fisher Scientific # 34076) and images were obtained using a ChemiDoc Imaging System (Bio-Rad laboratory, Inc.). Densitometry data were collected using Image Lab (Bio-Rad laboratory, Inc., Version 6.0) and results were analyzed using Graph Pad Prism software.

Cell lines: mTERT-immortalized mouse CCD cells (5, 6) were cultured in 1:1 DMEM/F-12 (Gibco GlutaMAX™; Fisher #10565018) with 5% FBS (Gibco One Shot™; Fisher #A3160602) and

Penicillin/Streptomycin (Mediatech, Inc., Corning 30-002). Complete cell culture medium was supplemented with dexamethasone (0.2 µg/ml; Sigma #D8893-1mg), triiodothrionine (10 nM; Sigma #T5616-1mg), 1x insulin-transferrin-sodium selenite (Sigma #I1884-1VL), and L-Glutamine (200mM; Corning Cellgro #25-005-CI).

Real-time PCR analysis: Relative quantification of *Pkhd1* mRNA in cells was performed using the delta-T method (58) using the following primer sets from Integrated DNA Technologies: *Pkhd1*-T forward 5'-CAGTTCTTGCCAGAGCATTTAC-3', *Pkhd1*-T reverse 5'-CAGAATCTCACCTCCTGCTATG-3', *Pkhd1*-M forward 5'-CTGATAATGCACAGGGACCTAC-3', *Pkhd1*-M reverse 5'-GGCAAAGGATGAAATGGAAGT G-3', *Pkhd1*-B forward 5'- CCA CCAGAAACCATCCAGTAA-3', *Pkhd1*-B reverse 5'- AGACCTCTCCTCTCCCATTT-3'. Relative *Pkhd1* mRNA levels from kidneys were determined by measuring *Pkhd1* ex66-67 expression normalized to *Ppia* (*peptidylpropyl isomerase A*); data are expressed as mean ± S.E; n=3 per group, using primers *Pkhd1* forward 5'-CCAGAAGACATATCTGAATCCCAGGC-3' (mPkhd1 e66F), reverse 5'-AGCAAGAGATCCTGGAACACAGGT-3' (mPkhd1 e67R), *Ppia* forward 5'-AGCACTGGAGAGAAAGGATT, reverse 5'- ATTATGGCGTGTAAAGTCACCA.

Antibodies: Primary antibodies used for WB analysis were produced against: FPC, (rat monoclonal (mAb), Baltimore PKD Center; PD1E1; 1:1000), cystin (rabbit, polyclonal (pAb), 70053; 1:500) (14, 15), PKD2 (rabbit mAb, Baltimore PKD Center; 3374; 1:1000), β-actin (mouse, mAb, Santa Cruz; sc-47778; 1:3000), Ift88 (rabbit pAb, GN593; 1:500) (59), GAPDH (rabbit pAb, Abcam; ab9485; 1:1000), p62/SQSTM1 (mouse mAb, R&D Systems; MAB8028; 1:1000), pan-polyubiquitin (rabbit pAb, Biomol: UG9510; 1:1000), polyubiquitin K63 (rabbit mAb, Millipore; 05-1308; 1:1000), polyubiquitin K48 (rabbit pAb, Cell Signaling; 4289; 1:1000), ENaCα (rabbit pAb, StressMarq; SPC-403; 1:1000). ENaCα (goat pAb, Santa Cruz; sc-22239; 1:200), LAMP1 (mouse mAb: Sztul Lab; 1:20 (60)).

Western blotting: Cells were lysed in RIPA buffer (Pierce; Thermo #89901) containing protease and phosphatase inhibitors (Halt; Thermo #1861281), sonicated, and centrifuged at 12000 rpm

for 30 min. The supernatant was collected, and protein concentration measured using a BCA Protein Assay (Pierce; Thermo # 23225). Equal amounts of proteins were denatured using NuPAGE reducing agent (Invitrogen; Thermo #NP0009), separated by SDS-PAGE using NuPAGE 4-12% bis-tris gel (Invitrogen; Thermo #WG1402BOX) or 3-8% tris-acetate gel (Invitrogen; Thermo #WG1602BOX), and electro-transferred to a nitrocellulose membrane (Odyssey; Li-Cor #926-31092). Membranes were incubated with primary antibodies overnight at 4 ºC and secondary antibodies (Li-Cor; 1:20000) for 1 hour at room temperature. Results were imaged using a Li-Cor Odyssey CLx imaging system.

Statistical analysis: Densitometry was performed using ImageStudio Lite software. Results were transferred to GraphPad Prism and data subject to Student's t-test or ANOVA analysis using GraphPad Software.

Immunocytochemistry and confocal microscopy: Cells were seeded on glass coverslips pretreated with HistoGrip (Fisher #008050) to enhance cell adhesion. After reaching approx. 60% confluence, the cells were washed with PBS, fixed with 4% paraformaldehyde, quenched with ammonium chloride, permeabilized with 0.1% Triton X-100, blocked with 2.5% goat serum, incubated with primary antibodies and Alexa Fluor-conjugated secondary antibodies (1:500), stained with Hoechst 33258 or DAPI, and mounted onto glass microscope slides. Following each step, the cells were washed with PBS. Imaging was done using a Nikon A1R Confocal Microscope and Advanced NIS-Elements software.

Patch Clamp: Whole cell voltage-clamp recordings were performed on *wt* and *cpk* cells at 24 to 32 hours after seeding on plastic coverslips in regular gro*wt*h medium as previously described (53, 54). Briefly, cells were bathed in an external solution containing (in mM): 145 NaCl, 2.7 KCl, 1.8 CaCl2, 2 MgCl2, 5.5 glucose, and 10 HEPES, pH 7.4 and continuously perfused (~3 ml/min). Patch pipette resistance was 2.5-3 MΩ when filled with an internal solution containing (in mM): 135 potassium glutamic acid, 10 KCl, 6 NaCl, 1 Mg2ATP, 5.5 glucose, 10 HEPES and 0.5 EGTA, pH 7.3. Junction potentials were considered and corrected before breaking the cell membrane

and the formation of a whole-cell patch. To acquire individual cell capacitance, a transient current was induced by applying a short (15 ms) depolarization pulse from -30 to -20 mV before whole-cell current recording. To measure amiloride sensitive currents in voltage clamp, 10 μM amiloride was applied after recording control current. Whole-cell currents were evoked using a voltage step protocol from -90 to 30 mV in 20 mV increments of 450 ms duration at 5 s intervals. The cell membrane potential was held at -30 mV during recording. Signals from whole-cell recording were filtered and sampled at 2 kHz. Current voltage (I-V) relationships were constructed by measuring the steady-state current values at the end of each voltage step. Data acquisition and analysis were performed using Axonpatch 200B amplifier, Digidata 1322A analog-to-digital converter, pClamp 9.2 software (Axon Instruments/Molecular Devices, USA) and Origin Software (Microcal Software, Northampton, MA). All experiments were performed at room temperature.

AUTHOR CONTRIBUTIONS

Yiming Zhang contributed to experimental design, performed most of the experimental procedures, contributed to data analysis and manuscript writing. **Chaoze Yang** designed experiments, prepared samples, and performed western blotting analysis of cystin and FPC expression in mouse kidneys. **Wei Wang** designed, performed, and analyzed the patch clamp studies. **Naoe Harafui** designed the experiments and performed and analyzed mRNA expression levels in cells and kidney tissues. **P. Darwin Bell** developed the immortalized cell lines and helped to interpret initial results. **Lisa M. Guay-Woodford** supervised studies in *wt* and *cpk* mice, contributed to the interpretation of results and manuscript writing. **Zsuzsanna Bebok** conceived the study, co-designed the majority of the experiments, supervised the analysis and presentation of experimental results, and wrote the manuscript.

Acknowledgments: We thank Dr. Adam Richman for critical reading and help with editing of the manuscript.

Funding: UAB HRFD Core Center and O'Brien Center for Acute Kidney Injury Center Pilot Program (ZsB) P30DK072482, UAB CF Research and Translation Core Center and CCF-ROWE19RO, UAB Research and Development Program (ZsB and WW); R01DK121530, PKD Foundation, and The Moran Family Foundation (LGW).

REFERENCES

1. Preminger, G. M., Koch, W. E., Fried, F. A., McFarland, E., Murphy, E. D., and Mandell, J. (1982) Murine congenital polycystic kidney disease: a model for studying development of cystic disease. *J Urol* **127**, 556-560
2. Schieren, G., Pey, R., Bach, J., Hafner, M., and Gretz, N. (1996) Murine models of polycystic kidney disease. *Nephrol Dial Transplant* **11 Suppl 6**, 38-45
3. Guay-Woodford, L. M. (2003) Murine models of polycystic kidney disease: molecular and therapeutic insights. *Am J Physiol Renal Physiol* **285**, F1034-1049
4. Yang, C., Harafuji, N., O'Connor, A., Kesterson, R., Watts, J., Majmundar, A., Braun, D., Lek, M., Laricchia, K., Fath, H., Mane, S., Shril, S., Hildebrandt, F., and Guay-Woodford, L. (2021) Cystin genetic variants cause autosomal recessive polycystic kidney disease associated with altered Myc expression. *Scientific Reports* **11**
5. Hwang, V. J., Kim, J., Rand, A., Yang, C., Sturdivant, S., Hammock, B., Bell, P. D., Guay-Woodford, L. M., and Weiss, R. H. (2015) The cpk model of recessive PKD shows glutamine dependence associated with the production of the oncometabolite 2-hydroxyglutarate. *Am J Physiol Renal Physiol* **309**, F492-498
6. Steele, S. L., Wu, Y., Kolb, R. J., Gooz, M., Haycraft, C. J., Keyser, K. T., Guay-Woodford, L., Yao, H., and Bell, P. D. (2010) Telomerase immortalization of principal cells from mouse collecting duct. *Am J Physiol Renal Physiol* **299**, F1507-1514
7. Hou, X., Mrug, M., Yoder, B. K., Lefkowitz, E. J., Kremmidiotis, G., D'Eustachio, P., Beier, D. R., and Guay-Woodford, L. M. (2002) Cystin, a novel cilia-associated protein, is disrupted in the cpk mouse model of polycystic kidney disease. *J Clin Invest* **109**, 533-540
8. Yoder, B. K., Hou, X., and Guay-Woodford, L. M. (2002) The polycystic kidney disease proteins, polycystin-1, polycystin-2, polaris, and cystin, are co-localized in renal cilia. *J Am Soc Nephrol* **13**, 2508-2516

9. Udenwobele, D. I., Su, R. C., Good, S. V., Ball, T. B., Varma Shrivastav, S., and Shrivastav, A. (2017) Myristoylation: An Important Protein Modification in the Immune Response. *Front Immunol* **8**, 751

10. Wright, M. H., Heal, W. P., Mann, D. J., and Tate, E. W. (2010) Protein myristoylation in health and disease. *J Chem Biol* **3**, 19-35

11. Kahn, R. A., Goddard, C., and Newkirk, M. (1988) Chemical and immunological characterization of the 21-kDa ADP-ribosylation factor of adenylate cyclase. *J Biol Chem* **263**, 8282-8287

12. Franco, M., Chardin, P., Chabre, M., and Paris, S. (1996) Myristoylation-facilitated binding of the G protein ARF1GDP to membrane phospholipids is required for its activation by a soluble nucleotide exchange factor. *J Biol Chem* **271**, 1573-1578

13. Kaczmarek, B., Verbavatz, J. M., and Jackson, C. L. (2017) GBF1 and Arf1 function in vesicular trafficking, lipid homoeostasis and organelle dynamics. *Biol Cell* **109**, 391-399

14. Tao, B., Bu, S., Yang, Z., Siroky, B., Kappes, J. C., Kispert, A., and Guay-Woodford, L. M. (2009) Cystin localizes to primary cilia via membrane microdomains and a targeting motif. *J Am Soc Nephrol* **20**, 2570-2580

15. Wu, M., Yang, C., Tao, B., Bu, S., and Guay-Woodford, L. M. (2013) The ciliary protein cystin forms a regulatory complex with necdin to modulate Myc expression. *PLoS One* **8**, e83062

16. Parrot, C., Kurbegovic, A., Yao, G., Couillard, M., Cote, O., and Trudel, M. (2019) c-Myc is a regulator of the PKD1 gene and PC1-induced pathogenesis. *Hum Mol Genet* **28**, 751-763

17. Trudel, M. (2015) c-Myc Signalling in the Genetic Mechanism of Polycystic Kidney Disease. In *Polycystic Kidney Disease* (Li, X., ed), Brisbane (AU)

18. O'Connnor AK, G.-W. L. (2016) *The Polycystic Kidney Diseases and Other Hepato-Renal Fibrocystic Diseases: Clinical Phenotypes, Molecular Pathobiology, and Variation Between Mouse and Man* Elsevier

19. Goggolidou, P., and Richards, T. (2022) The genetics of Autosomal Recessive Polycystic Kidney Disease (ARPKD). *Biochim Biophys Acta Mol Basis Dis* **1868**, 166348

20. Kaimori, J. Y., Lin, C. C., Outeda, P., Garcia-Gonzalez, M. A., Menezes, L. F., Hartung, E. A., Li, A., Wu, G., Fujita, H., Sato, Y., Nakanuma, Y., Yamamoto, S., Ichimaru, N., Takahara, S., Isaka, Y., Watnick, T., Onuchic, L. F., Guay-Woodford, L. M., and Germino, G. G. (2017) NEDD4-family E3 ligase dysfunction due to PKHD1/Pkhd1 defects suggests a mechanistic model for ARPKD pathobiology. *Sci Rep* **7**, 7733

21. Eaton, D. C., Malik, B., Bao, H. F., Yu, L., and Jain, L. (2010) Regulation of epithelial sodium channel trafficking by ubiquitination. *Proc Am Thorac Soc* **7**, 54-64

22. Dorval, G., Boyer, O., Couderc, A., Delbet, J. D., Heidet, L., Debray, D., Krug, P., Girard, M., Llanas, B., Charbit, M., Krid, S., Biebuyck, N., Fila, M., Courivaud, C., Tilley, F., Garcelon, N., Blanc, T., Chardot, C., Salomon, R., and Lacaille, F. (2021) Long-term kidney and liver outcome in 50 children with autosomal recessive polycystic kidney disease. *Pediatr Nephrol* **36**, 1165-1173

23. Guay-Woodford, L. M. (2014) Autosomal recessive polycystic kidney disease: the prototype of the hepato-renal fibrocystic diseases. *J Pediatr Genet* **3**, 89-101

24. Rotin, D., and Staub, O. (2012) Nedd4-2 and the regulation of epithelial sodium transport. *Front Physiol* **3**, 212

25. Nesterov, V., Dahlmann, A., Krueger, B., Bertog, M., Loffing, J., and Korbmacher, C. (2012) Aldosterone-dependent and -independent regulation of the epithelial sodium channel (ENaC) in mouse distal nephron. *Am J Physiol Renal Physiol* **303**, F1289-1299

26. Wang, S., Zhang, J., Nauli, S. M., Li, X., Starremans, P. G., Luo, Y., Roberts, K. A., and Zhou, J. (2007) Fibrocystin/polyductin, found in the same protein complex with polycystin-2, regulates calcium responses in kidney epithelia. *Mol Cell Biol* **27**, 3241-3252

27. Demishtein, A., Fraiberg, M., Berko, D., Tirosh, B., Elazar, Z., and Navon, A. (2017) SQSTM1/p62-mediated autophagy compensates for loss of proteasome polyubiquitin recruiting capacity. *Autophagy* **13**, 1697-1708

28. Pan, B., Li, J., Parajuli, N., Tian, Z., Wu, P., Lewno, M. T., Zou, J., Wang, W., Bedford, L., Mayer, R. J., Fang, J., Liu, J., Cui, T., Su, H., and Wang, X. (2020) The Calcineurin-TFEB-p62 Pathway Mediates the Activation of Cardiac Macroautophagy by Proteasomal Malfunction. *Circ Res* **127**, 502-518

29. Su, H., and Wang, X. (2020) Proteasome malfunction activates the PPP3/calcineurin-TFEB-SQSTM1/p62 pathway to induce macroautophagy in the heart. *Autophagy* **16**, 2114-2116

30. Pampliega, O., and Cuervo, A. M. (2016) Autophagy and primary cilia: dual interplay. *Curr Opin Cell Biol* **39**, 1-7

31. Pampliega, O., Orhon, I., Patel, B., Sridhar, S., Diaz-Carretero, A., Beau, I., Codogno, P., Satir, B. H., Satir, P., and Cuervo, A. M. (2013) Functional interaction between autophagy and ciliogenesis. *Nature* **502**, 194-200

32. Albornoz, N., Bustamante, H., Soza, A., and Burgos, P. (2019) Cellular Responses to Proteasome Inhibition: Molecular Mechanisms and Beyond. *Int J Mol Sci* **20**

33. Bjorkoy, G., Lamark, T., Brech, A., Outzen, H., Perander, M., Overvatn, A., Stenmark, H., and Johansen, T. (2005) p62/SQSTM1 forms protein aggregates degraded by autophagy and has a protective effect on huntingtin-induced cell death. *J Cell Biol* **171**, 603-614

34. Bjorkoy, G., Lamark, T., and Johansen, T. (2006) p62/SQSTM1: a missing link between protein aggregates and the autophagy machinery. *Autophagy* **2**, 138-139

35. Lamark, T., Svenning, S., and Johansen, T. (2017) Regulation of selective autophagy: the p62/SQSTM1 paradigm. *Essays Biochem* **61**, 609-624

36. Matsumoto, G., Wada, K., Okuno, M., Kurosawa, M., and Nukina, N. (2011) Serine 403 phosphorylation of p62/SQSTM1 regulates selective autophagic clearance of ubiquitinated proteins. *Mol Cell* **44**, 279-289

37. Mori, Y., Mori, T., Wakabayashi, M., Yoshizaki, Y., Zeniya, M., Sohara, E., Rai, T., and Uchida, S. (2015) Involvement of selective autophagy mediated by p62/SQSTM1 in KLHL3-dependent WNK4 degradation. *Biochem J* **472**, 33-41

38. Pankiv, S., Clausen, T. H., Lamark, T., Brech, A., Bruun, J. A., Outzen, H., Overvatn, A., Bjorkoy, G., and Johansen, T. (2007) p62/SQSTM1 binds directly to Atg8/LC3 to facilitate degradation of ubiquitinated protein aggregates by autophagy. *J Biol Chem* **282**, 24131-24145

39. Nagaoka, U., Kim, K., Jana, N. R., Doi, H., Maruyama, M., Mitsui, K., Oyama, F., and Nukina, N. (2004) Increased expression of p62 in expanded polyglutamine-expressing cells and its association with polyglutamine inclusions. *J Neurochem* **91**, 57-68

40. Mauthe, M., Orhon, I., Rocchi, C., Zhou, X., Luhr, M., Hijlkema, K. J., Coppes, R. P., Engedal, N., Mari, M., and Reggiori, F. (2018) Chloroquine inhibits autophagic flux by decreasing autophagosome-lysosome fusion. *Autophagy* **14**, 1435-1455

41. Fedele, A. O., and Proud, C. G. (2020) Chloroquine and bafilomycin A mimic lysosomal storage disorders and impair mTORC1 signalling. *Biosci Rep* **40**

42. Klionsky, D. J., Elazar, Z., Seglen, P. O., and Rubinsztein, D. C. (2008) Does bafilomycin A1 block the fusion of autophagosomes with lysosomes? *Autophagy* **4**, 849-850

43. Mauvezin, C., and Neufeld, T. P. (2015) Bafilomycin A1 disrupts autophagic flux by inhibiting both V-ATPase-dependent acidification and Ca-P60A/SERCA-dependent autophagosome-lysosome fusion. *Autophagy* **11**, 1437-1438

44. Wurzer, B., Zaffagnini, G., Fracchiolla, D., Turco, E., Abert, C., Romanov, J., and Martens, S. (2015) Oligomerization of p62 allows for selection of ubiquitinated cargo and isolation membrane during selective autophagy. *Elife* **4**, e08941

45. Wang, Y., Argiles-Castillo, D., Kane, E. I., Zhou, A., and Spratt, D. E. (2020) HECT E3 ubiquitin ligases - emerging insights into their biological roles and disease relevance. *J Cell Sci* **133**

46. Dikic, I. (2017) Proteasomal and Autophagic Degradation Systems. *Annu Rev Biochem* **86**, 193-224

47. Newton, K., Matsumoto, M. L., Wertz, I. E., Kirkpatrick, D. S., Lill, J. R., Tan, J., Dugger, D., Gordon, N., Sidhu, S. S., Fellouse, F. A., Komuves, L., French, D. M., Ferrando, R. E., Lam, C., Compaan, D., Yu, C., Bosanac, I., Hymowitz, S. G., Kelley, R. F., and Dixit, V. M. (2008) Ubiquitin chain editing revealed by polyubiquitin linkage-specific antibodies. *Cell* **134**, 668-678

48. Butterworth, M. B. (2010) Regulation of the epithelial sodium channel (ENaC) by membrane trafficking. *Biochim Biophys Acta* **1802**, 1166-1177

49. Pratt, J. H. (2005) Central role for ENaC in development of hypertension. *J Am Soc Nephrol* **16**, 3154-3159

50. Goto, M., Hoxha, N., Osman, R., and Dell, K. M. (2010) The renin-angiotensin system and hypertension in autosomal recessive polycystic kidney disease. *Pediatr Nephrol* **25**, 2449-2457

51. Liu, L., Duke, B. J., Malik, B., Yue, Q., and Eaton, D. C. (2009) Biphasic regulation of ENaC by TGF-{alpha} and EGF in renal epithelial cells. *Am J Physiol Renal Physiol* **296**, F1417-1427

52. Malik, B., Price, S. R., Mitch, W. E., Yue, Q., and Eaton, D. C. (2006) Regulation of epithelial sodium channels by the ubiquitin-proteasome proteolytic pathway. *Am J Physiol Renal Physiol* **290**, F1285-1294

53. Lazrak, A., Jurkuvenaite, A., Chen, L., Keeling, K. M., Collawn, J. F., Bedwell, D. M., and Matalon, S. (2011) Enhancement of alveolar epithelial sodium channel activity with decreased cystic fibrosis transmembrane conductance regulator expression in mouse lung. *Am J Physiol Lung Cell Mol Physiol* **301**, L557-567

54. Lazrak, A., Samanta, A., and Matalon, S. (2000) Biophysical properties and molecular characterization of amiloride-sensitive sodium channels in A549 cells. *Am J Physiol Lung Cell Mol Physiol* **278**, L848-857

55. Pohl, C., and Dikic, I. (2019) Cellular quality control by the ubiquitin-proteasome system and autophagy. *Science* **366**, 818-822

56. Rocco, M. V., Neilson, E. G., Hoyer, J. R., and Ziyadeh, F. N. (1992) Attenuated expression of epithelial cell adhesion molecules in murine polycystic kidney disease. *Am J Physiol* **262**, F679-686

57. Taub, M., Laurie, G. W., Martin, G. R., and Kleinman, H. K. (1990) Altered basement membrane protein biosynthesis by primary cultures of cpk/cpk mouse kidney. *Kidney Int* **37**, 1090-1097

58. Livak, K. J., and Schmittgen, T. D. (2001) Analysis of relative gene expression data using real-time quantitative PCR and the 2(-Delta Delta C(T)) Method. *Methods* **25**, 402-408

59. Taulman, P. D., Haycraft, C. J., Balkovetz, D. F., and Yoder, B. K. (2001) Polaris, a protein involved in left-right axis patterning, localizes to basal bodies and cilia. *Mol Biol Cell* **12**, 589-599

60. Nelson, D. S., Alvarez, C., Gao, Y. S., Garcia-Mata, R., Fialkowski, E., and Sztul, E. (1998) The membrane transport factor TAP/p115 cycles between the Golgi and earlier secretory compartments and contains distinct domains required for its localization and function. *J Cell Biol* **143**, 319-331

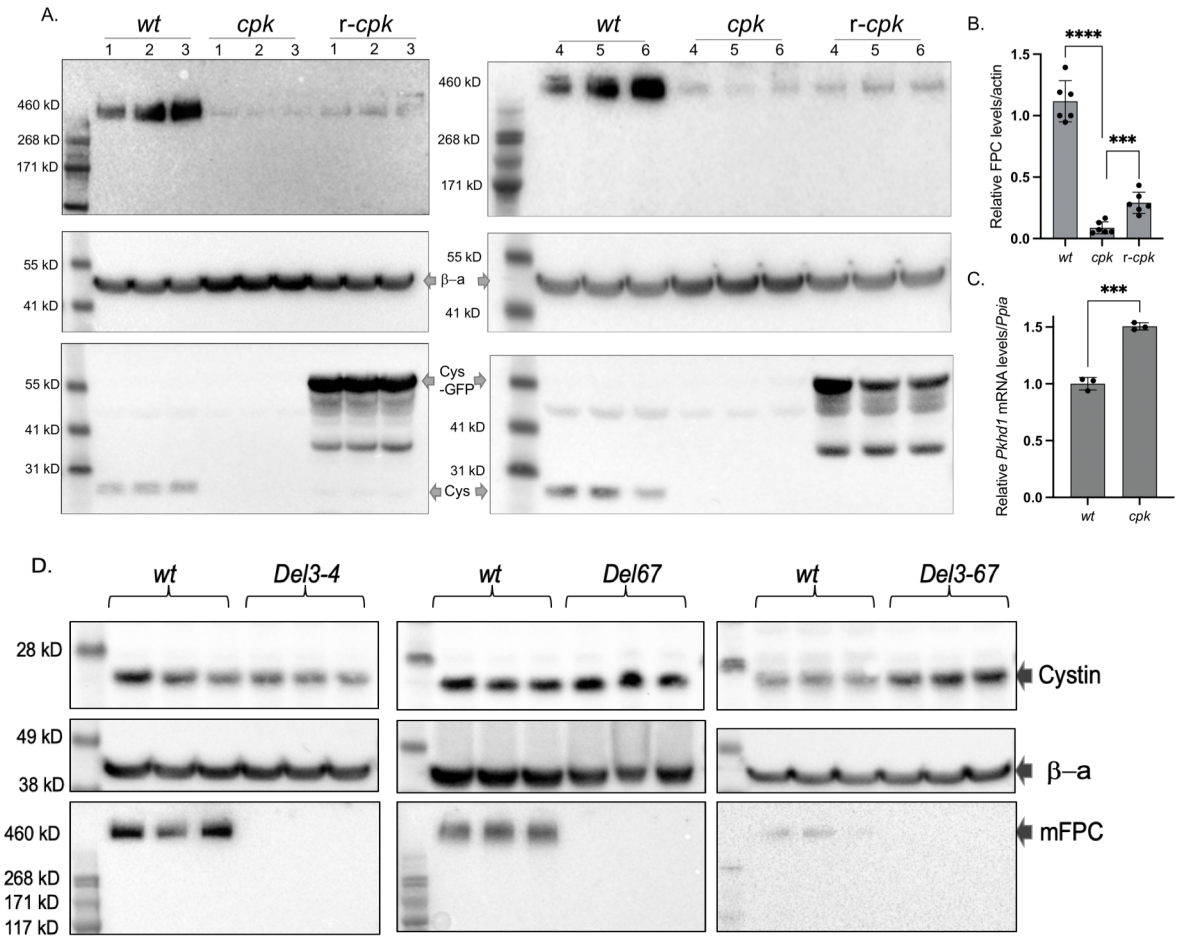

Fig.1 **Reduced FPC levels in *cpk* mouse kidneys and partial rescue in r-*cpk*. A:** Kidney lysates from *wt* (C57BL/6), *cpk* and r-*cpk* mouse kidneys were analyzed in duplicate WB experiments using an anti-FPC antibody recognizing the C-terminal region of the mouse protein and an anti-cystin (rabbit) antibody. **B:** FPC levels are plotted relative to β-actin. ****: $p<0.0001$, ***: $p<0.0005$. **C:** *Pkhd1* mRNA levels were measured by real time RT-PCR. *Cpk* mice expressed more *Pkhd1* mRNA than *wt*. ***: $p<0.001$. **D:** Kidney lysates from *Pkhd1* mutant mouse kidneys (*Del3-4, Del67 and Del3-67*) were tested for cystin and FPC expression, n=3. Cystin expression was not affected by the loss of FPC.

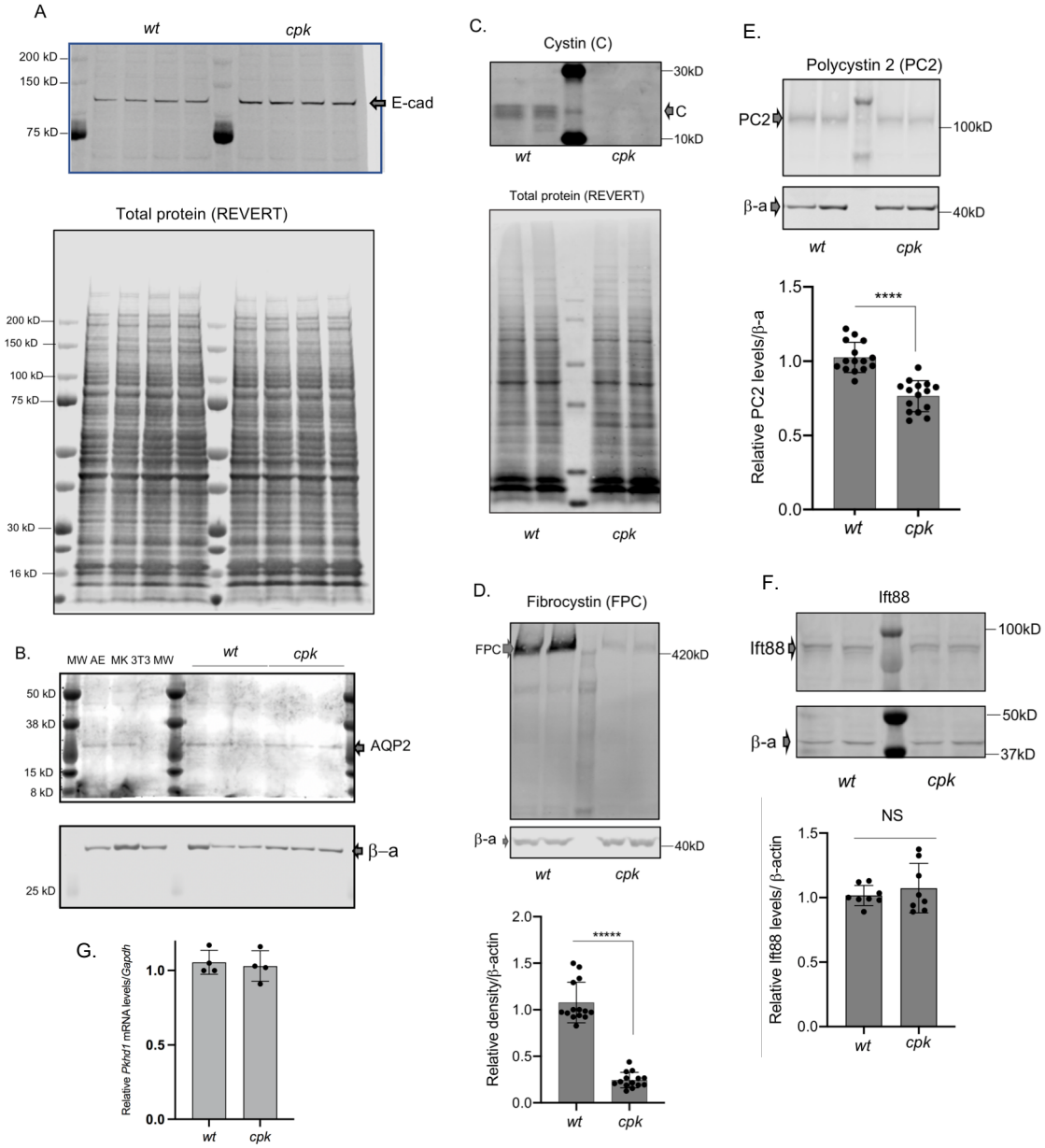

Fig.2. **Reduced FPC levels in *cpk* cells. A-B:** Characterization of *wt* and *cpk* cell lines, n=4. **A:** E-cadherin (E-cad) expression tested as an epithelial marker in, n=4. **B:** Aquaporin-2 (AQP2) expression as a CCD marker. AE: airway epithelial cells, MK: mixed mouse kidney epithelial cells, 3T3: mouse fibroblast cell line. **C:** *Cpk* cells lack cystin. Cystin is only present in *wt* cells. Cystin was detected using lab a rabbit polyclonal anti-cystin antibody. Total protein stain (REVERT) of the same gel is presented in the lower panel. **D.** *Cpk* cells had less FPC than *wt*. 30 ug of total protein analyzed by WB using an anti-FPC monoclonal antibody. Relative FPC abundance was quantitatively assessed by densitometry and expressed relative to β-actin (N=8, n=2, ******: p<0.00001)). **E:** Pc2 was reduced in *cpk* cells. PC2 WB using a rabbit polyclonal PC2 antiserum. PC2 abundance was quantitatively assessed by densitometry and expressed relative to β-actin. (N=8, n=2, ****: p<0.0001. **F:** Ift88 levels were similar in *wt* and *cpk* cells. Ift88 was detected using anti-Ift88 rabbit polyclonal antiserum. No significant differences were observed based on quantitative assessment of densitometry expressed relative to β-actin (N=4, n=2). **G.** *Pkhd1* mRNA levels in *wt* and *cpk* cells. Plotted values indicate mRNA levels in four independently-derived samples (n=4). No significant differences were observed (NS).

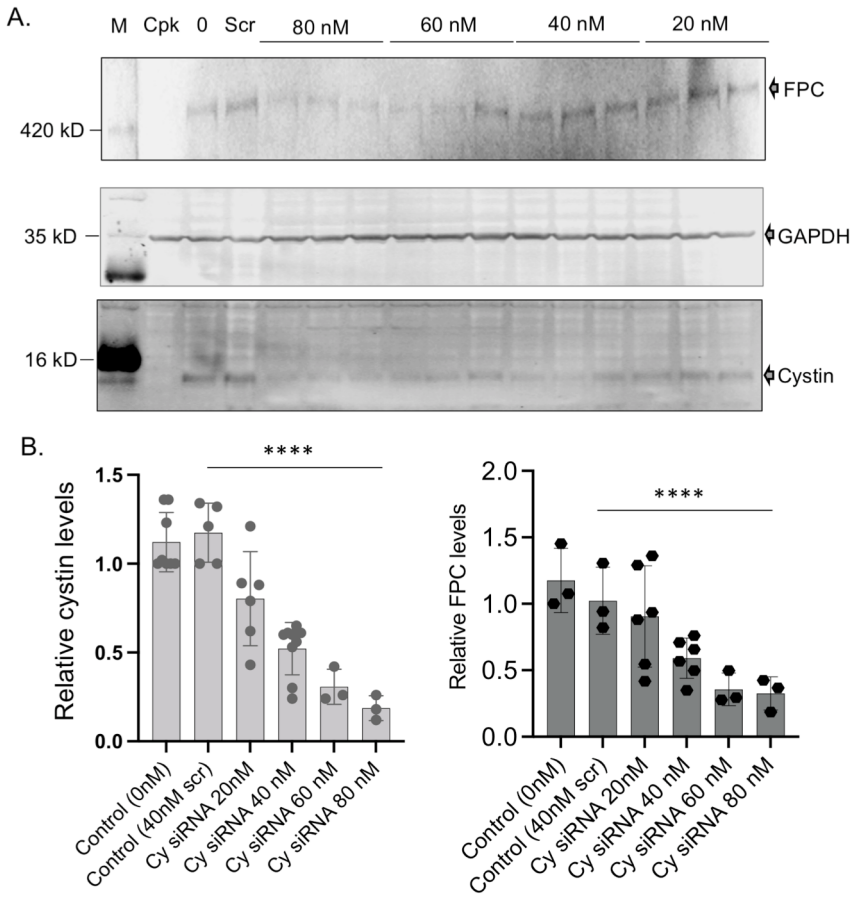

Fig.3. **siRNA-based cystin depletion leads to FPC reduction. A:** Representative WB of FPC (top) and cystin (bottom) following cystin siRNA treatment for 72 hours (siRNA concentrations indicated above image). GAPDH levels (middle) were used to normalize cystin and FPC expression. **B:** Quantitation of cystin siRNA results from densitometric analysis. Values are relative to GAPDH internal control from n=1-3 separate experiments, with n=3-6 under each siRNA concentration. ****$p<0.0001$ significance between scrambled and cystin-specific siRNA (80 nM).

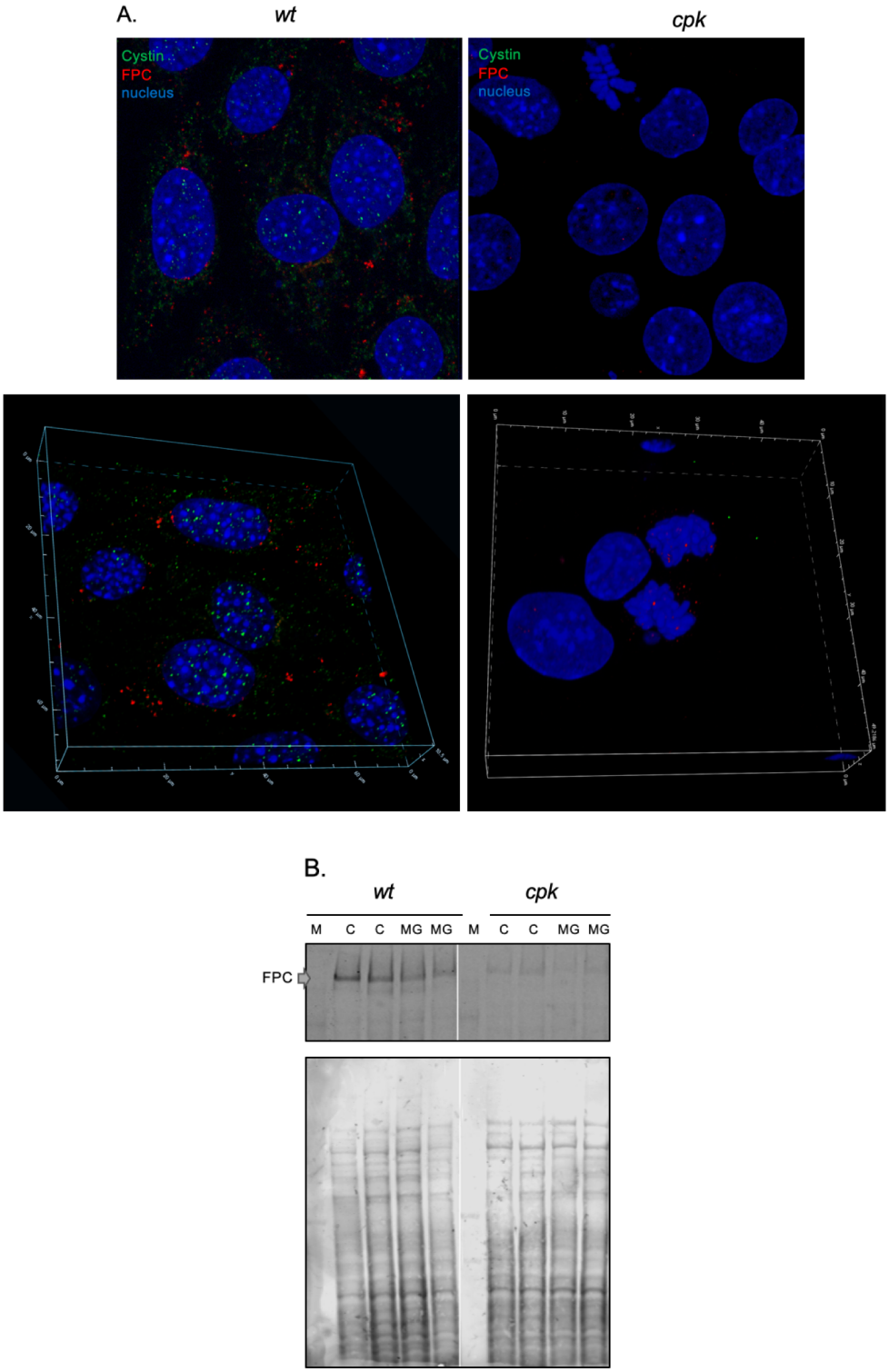

Fig.4. **No cystin and FPC co-localization in *wt* cells, and minimal FPC staining in *cpk* cells lacking cystin. A:** Representative images of *wt* and *cpk* cells at top with 3D reconstituted images at bottom. Note cystin in nuclei of *wt* cells and minimal FPC staining in *cpk* cells. **B: Proteasome inhibition did not rescue FPC in *wt* or *cpk* cells.** Cells were treated with MG132 for 4 hrs. and FPC was labeled as in Fig 2. Total cellular proteins are shown on the bottom gel. M: molecular weight marker; C: Control, untreated samples; MG: MG132 for 4 hrs. Arrow indicates full length FPC.

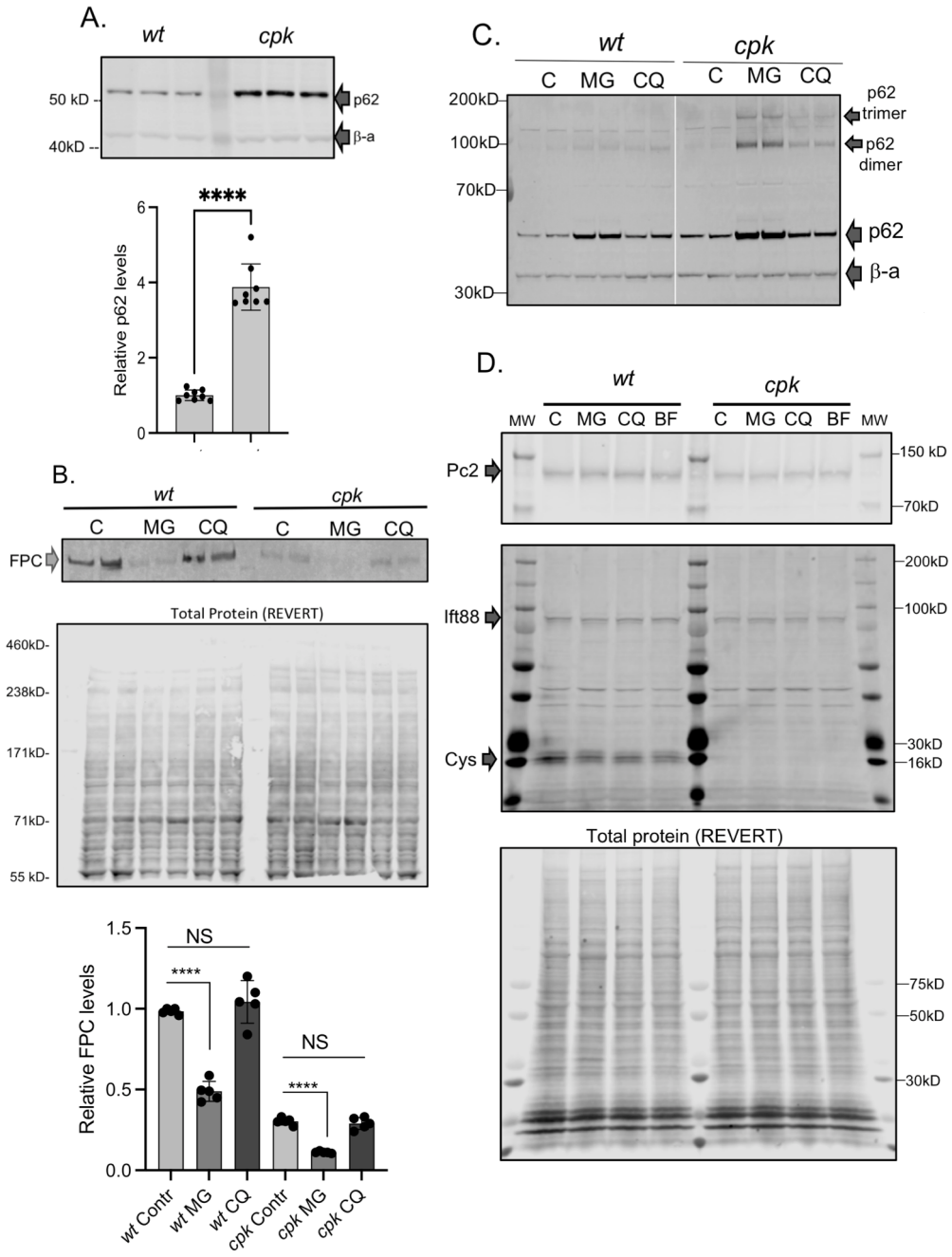

Fig.5. **Activation of selective autophagy leads to reduced FPC levels. A:** Enhanced SQSTM1/p62 levels in *cpk* compared to *wt* cells. Representative gel image on top. Relative p62 levels/β-actin plotted on bottom (N=2, n=4), ****: p<0.0001. **B: Proteasome inhibition led to reduced FPC in *wt* and *cpk* cells.** Top shows a representative gel image (n=3, n=2). Middle shows a total protein gel image (REVERT). Quantitation showing relative FPC levels/total protein shown at bottom. (N=3, n=2), ****: p<0.0001. **C: Hyperactivation of selective autophagy by PI, especially in *cpk* cells.** Representative gel image (n=2). C: control, MG: MG132 (PI), CQ: chloroquine (LI), and BF: bafilomycin (LI). **D: Pc2, Ift88 and cystin levels did not change in the presence of PI or LI.** Representative gel image for Pc2, Ift88 and cystin expression (C) (top and middle); Total protein pattern (REVERT, bottom).

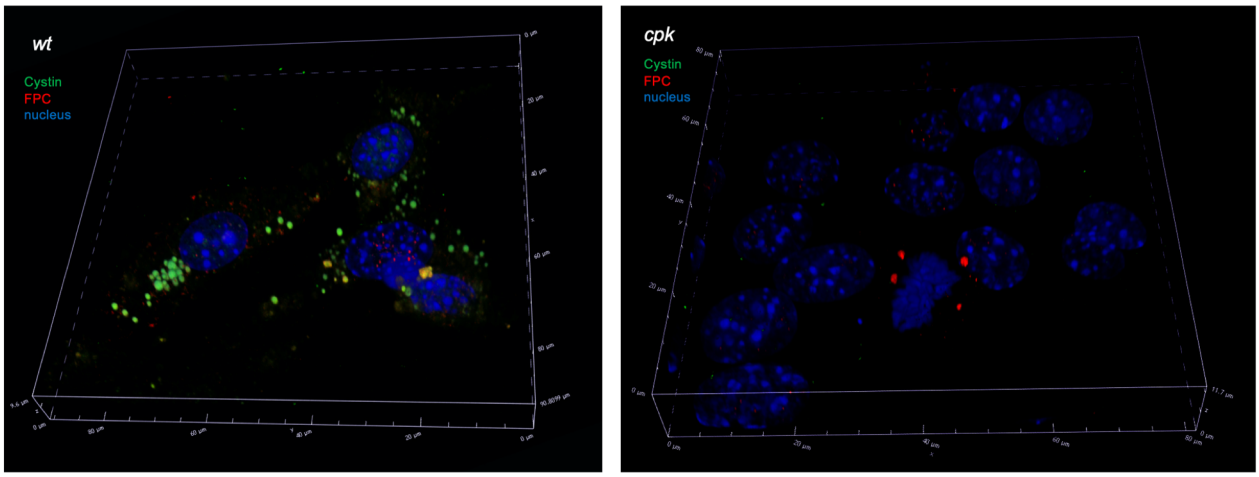

Fig.6. **Co-localization of cystin and FPC in cytoplasmic particles of *wt* cells following PI and LI.** *Wt* cells were stained with anti-cystin (green) and anti-FPC (red) antibodies following treatment with PI and LI for 8 hours, to facilitate formation of autophagic particles. Cystin colocalized with FPC in some particles (yellow staining). In cystin-negative *cpk* cells, aggregates of FPC were detected in some cells (right).

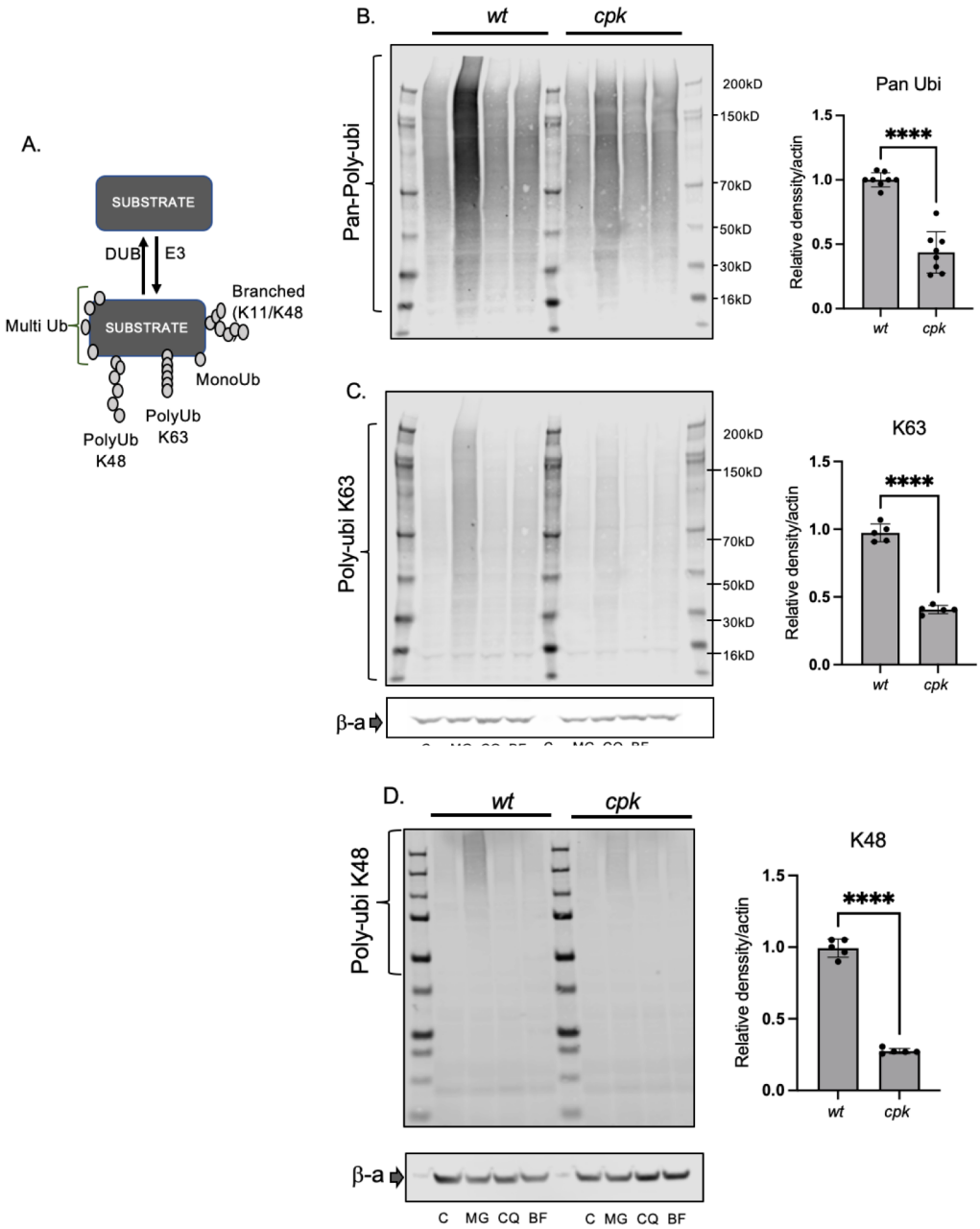

Fig.7. **Reduced polyubiquitination in *cpk* cells. A:** Scheme depicting types of ubiquitination. Proteins are polyubiquitinated prior to ERAD, lysosomal degradation or autophagy. The length of the poly-ubiquitin chain varies. **B-D:** Reduced polyubiquitination in *cpk* cells. Representative gels are shown for polyubiquitination of cellular proteins in control (C), PI (MG), and LI (CQ and BF)-treated cells. **B:** Pan-poly-ubiquitination; **C:** K63-linked; and **D:** K48-linked polyubiquitination. Results of densitometric analysis are plotted relative to b-actin levels (N=3, n=2), ****: $p<0.00001$.

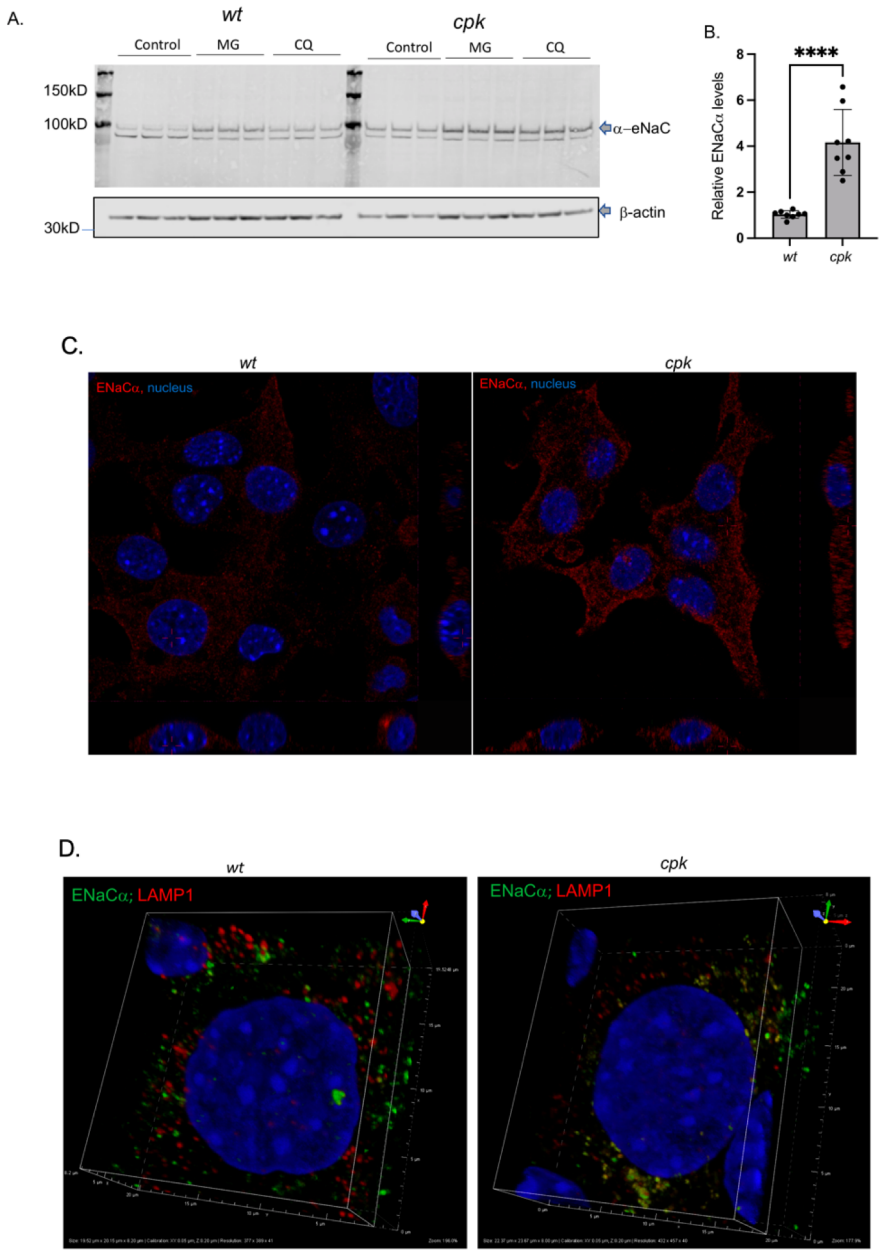

Fig.8. **Increased ENaCα in *cpk* cells. A:** Representative WB of ENaCα in *wt* and *cpk* cells. β-actin was used as a control. **B:** Cumulative plot of ENaCα levels (N=3 individual experiments, n=7; ***: p<0.0001). **C: Increased ENaC IF in *cpk* cells.** Confocal microscopy images of *wt* (left) and *cpk* cells (right). **D: Co-localization of ENaC and LAMP1.** ENaC was highly co-localized with LAMP 1 in *cpk* cells.

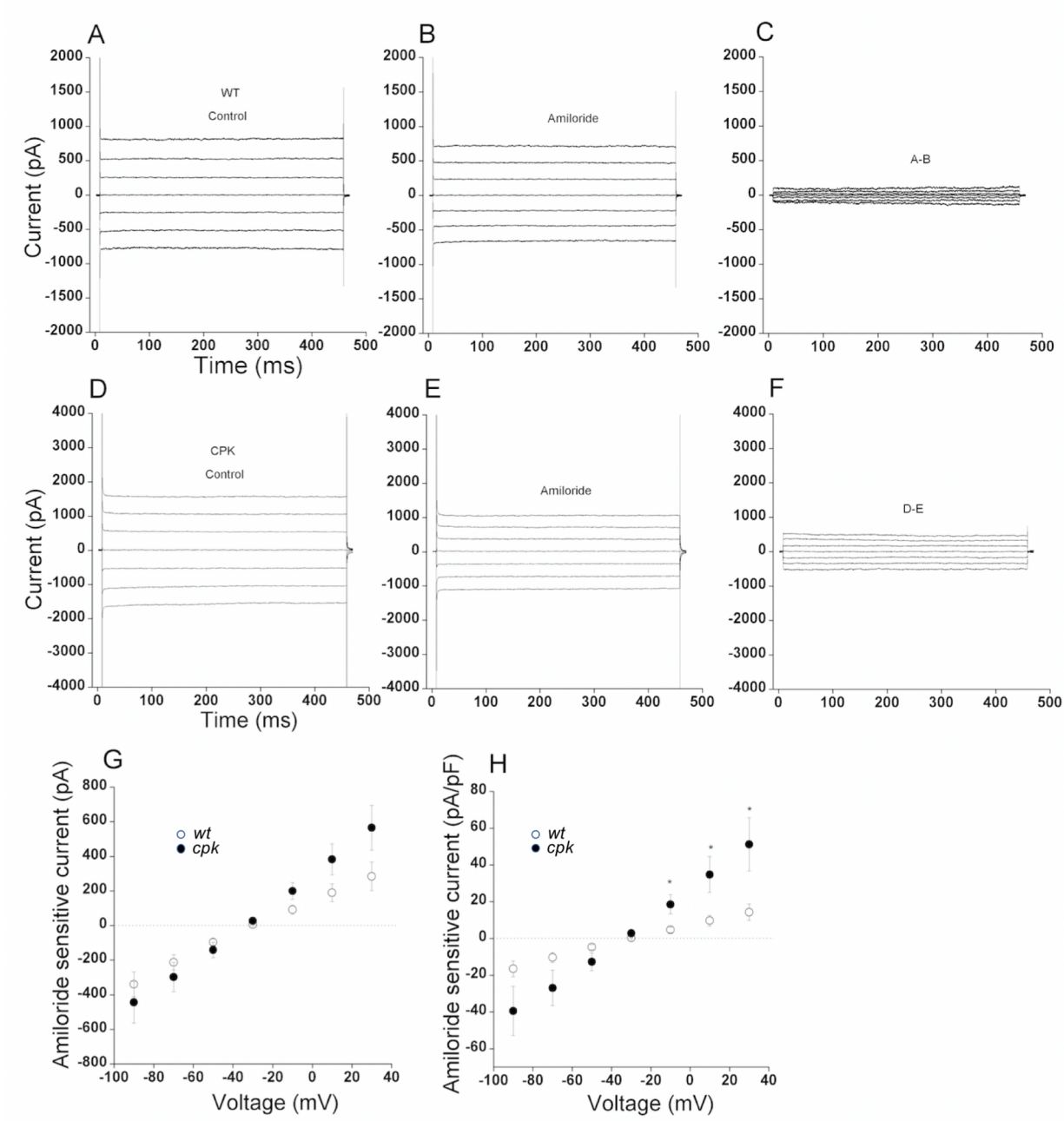

Fig.9. Higher relative amiloride sensitive currents in cpk compared to wt cells. Whole-cell currents were evoked by applying voltage steps from -90 to 30 mV in 20 mV increments. Cells were held at -30 mV. Representative whole-cell current recordings from *wt* **(A-C)** and *cpk* **(D-F)** cells in the absence **(A, D)** and presence **(B, E)** of amiloride (10 μM). Amiloride-sensitive currents (C and F) were measured by subtracting B from A and E from D. **(G)** Mean I-V relationship of amiloride-sensitive currents expressed by total currents for *wt* (open circle, n=15) and *cpk* (dark circle, n=13) cells. **(H)** Mean I-V relationship of amiloride-sensitive currents were expressed by current density for *wt* (open circle, n=15) and *cpk* (dark circle, n=13) cells. Values are means ±SE, *p<0.05.